Soft Matter

ARTICLE TYPE

Cite this: DOI: 00.0000/xxxxxxxxxx

Supplementary Informations for: On the role of Polydispersity on the Phase Diagram of Colloidal Rods

Carlo Andrea De Filippo[a], Sara Del Galdo,[a] Pietro Corsi,[a] Cristiano De Michele,*[b] and Barbara Capone*[a]

1 Numerical Details

NPT Monte Carlo (MC) simulations are performed on systems made of $N = 1296$ particles for the Isotropic phase, and $N = 2400$ colloids for the phases that are expected to be ordered (see Appendix 2).

Each MC step consists either in a volume move, a change in either position or orientation of one particle. Each volume move has a $1/N$ probability, translational or rotational moves are equally probable. Volume moves consists in the random selection and variation of one of the box sides. The random selection induces anisotropic changes in volume. Such an anisotropy is needed to avoid the introduction of artificial order in the system and to ease the formation of mesophases[1]. Periodic boundary conditions are used. Up to 6×10^6 MC steps have been performed to obtain the computational results, discarding the initial equilibration of the systems.

2 Initial configurations

To introduce polydispersity in the studied systems, the initial configurations were generated by combining HSCs of diverse lengths and/or diameters according to truncated or inverse truncated Gaussian probability distributions. We hence introduced the Polydispersity Index $PI_X = \Delta X/\bar{X}$, with $X = (L, D, A)$ and ΔX the maximum deviation from the average $\bar{X}$. The standard deviation $\sigma_X = \Delta X/1.177$ was chosen to have ΔX corresponding to the half width at half maximum of the Gaussian distributions. To study the low pressure phase space, four types of polydispersities, with either 0.5 or 0.75 as PI, were studied:

- L is modeled as a truncated Gaussian and D is uniform (G_L), A results as a truncated Gaussian ($PI_L = PI_A \in (0.5, 0.75)$);
- L is uniform and D is modeled as an inverse truncated Gaussian (IG_D), A results as a truncated Gaussian ($PI_A \in (0.5, 0.75)$);
- L is uniform and D is modeled as a truncated Gaussian (G_D), A results as an inverse truncated Gaussian ($PI_D \in (0.5, 0.75)$);
- both L and D are modeled as truncated Gaussian ($G_{L,D}$), A results as an inverse truncated Gaussian ($PI_L = PI_D \in (0.5, 0.75)$).

For each case, $\bar{L}$ (or $\bar{D}$) is tuned in order to have $\bar{A} = \int P_d(D) P_l(L)(L/D)\, \mathrm{d}D\, \mathrm{d}L$ of fixed values.

To study the high pressure region of the phase space ($P^* > 1$), we narrowed the analysis to the first two cases (namely, G_L and IG_D) with $PI_A = 0.5$, which are representative of all the other ones.

In figure S1 the distributions employed to model the polydispersity for the case of $\bar{A} = 5$ and $PI = 0.5$ are reported.

For the low pressure cases ($P^* \leq 1$), the HSCs are initially arranged in a orthorhombic lattice by placing (18, 18, 4) particles for each side of the box (N=1296). The intermolecular distances are set as $\vec{a} = 1.01\,(D_{\max}, D_{\max}, L_{\max} + D_{\max})$, where $D_{\max}$ and $L_{\max}$ are the maximum diameter and length of the particles in the system (namely, $X_{\max} = \bar{X} + \Delta X$).

For the high pressure cases ($P^* > 1$), (20,20,6) HSCs are placed in a orthorhombic lattice (N=2400), as described before. Then, to ease the equilibration, particles are systematically moved closer till overlapping. In Fig. S2 are reported three examples of initial configurations of systems with $\bar{A} = 5$ at high pressure obtained via the aforementioned procedure.

3 Analysis of $\tilde{v}$

We report in table S1, the v_0, $\bar{v}_{\mathrm{excl}}$ and $\tilde{v}$ computed on the distributions described in the Appendix 2 (see equations 3, 11) for the $\bar{A} = 5$ systems.

We tested the dependence of $\tilde{v}$ upon the choice of the distribution used to model the polydispersity in length. To this aim, we chose two different distributions that are not symmetrical with

[a] Science Department, University of Roma Tre, Via della Vasca Navale 84, 00146, Rome, Italy; E-mail: barbara.capone@uniroma3.it.
[b] Physics Department, University of Roma "La Sapienza", Piazzale Aldo Moro 2, 00186, Rome, Italy; E-mail: cristiano.demichele@uniroma1.it

† Electronic Supplementary Information (ESI) available: [details of any supplementary information available should be included here]. See DOI: 10.1039/cXsm00000x/

‡ Additional footnotes to the title and authors can be included *e.g.* 'Present address:' or 'These authors contributed equally to this work' as above using the symbols: ‡, §, and ¶. Please place the appropriate symbol next to the author's name and include a `\footnotetext` entry in the the correct place in the list.

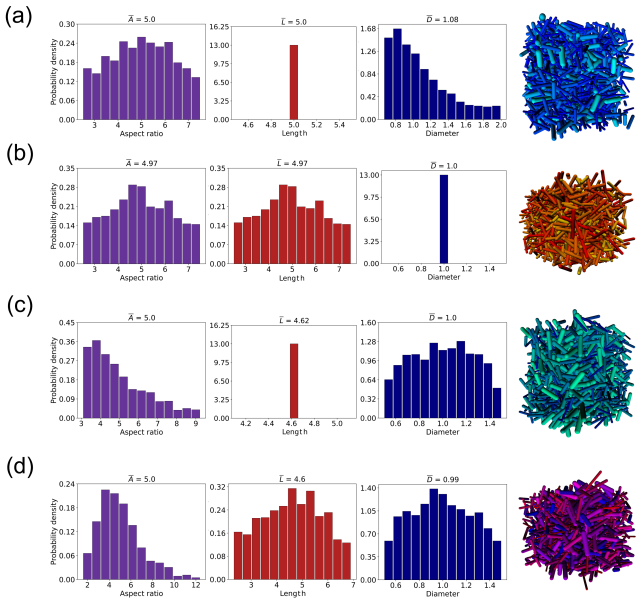

Fig. S1 Histograms of A, L and D values for the configurations of the simulated HSCs employed to model polydispersity in length, diameter or both, for the case of average aspect ratio equal to 5 with PI of 0.5. Snapshots of the corresponding equilibrium configurations at $P^* = 1$ are also reported. Panel (a) IG_D, panel (b) G_L, panel (c) G_D, panel (d) $G_{L,D}$.

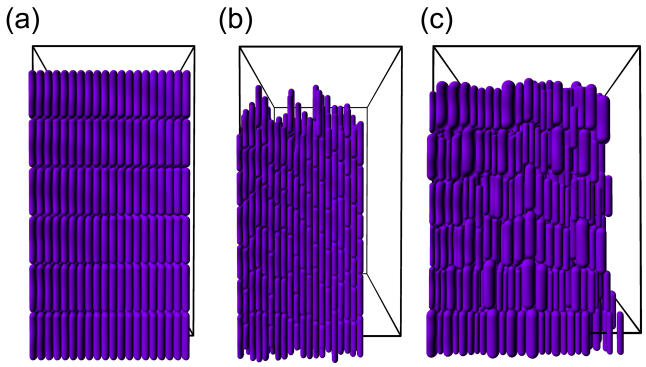

Fig. S2 Snapshots of the initial configuration of systems with $\bar{A} = 5$ for the monodisperse (a), G_L (b), and IG_D (c) cases after the compaction procedure.

respect to the average value of L; namely we employed an increasing and decreasing truncated linear distribution chosen so that the polydispersity $PI_L = 0.5$ so that $\bar{A} = 5$ (Case I and Case II, see S3). As reported in Table S2, while the values of $\bar{v}_0$ and $\bar{v}_{\text{excl}}$ vary for the different distributions, $\tilde{v}$ is always equal to the monodisperse corresponding case.

4 Isotropic EOS of the systems for all the elongations

In fig. S4 the EOS of the polydisperse systems studied at $P^* \leq 1$ (see Appendix 2) are reported for $\bar{A} = (1, 2, 2.5, 3, 4, 5)$. Fig. S5 shows the qualitative agreement between Parsons-Lee theory and simulations for the studied systems in the isotropic phase.

Table S1 $\bar{v}_{\text{excl}}$, $\bar{v}_0$ and $\tilde{v}$ computed analytically via Mathematica for the $\bar{A} = 5$ case (see Appendix 2 for the nomenclature of the system types)

System type	$\bar{v}_{\text{excl}}$	$\bar{v}_0$	$\tilde{v}$
Monodisperse	74.875	4.451	16.824
G_L $(PI = 0.5)$	74.875	4.451	16.824
G_L $(PI = 0.75)$	74.875	4.451	16.824
G_D $(PI = 0.5)$	68.334	4.517	15.128
$G_{L,D}$ $(PI = 0.5)$	68.334	4.517	15.128
IG_D $(PI = 0.5)$	86.725	5.835	14.863
G_D $(PI = 0.75)$	58.226	4.437	13.124
$G_{L,D}$ $(PI = 0.75)$	58.226	4.437	13.124
IG_D $(PI = 0.75)$	116.000	10.008	11.591

Table S2 $\bar{v}_{\text{excl}}$, $\bar{v}_0$ and $\tilde{v}$ computed analytically via Mathematica for $\bar{A} = 5$ when asymmetrical distributions are considered

System type	$\bar{v}_{\text{excl}}$	$\bar{v}_0$	$\tilde{v}$
Monodisperse	74.875	4.451	16.824
Case I	95.196	5.658	16.824
Case II	57.672	3.428	16.824

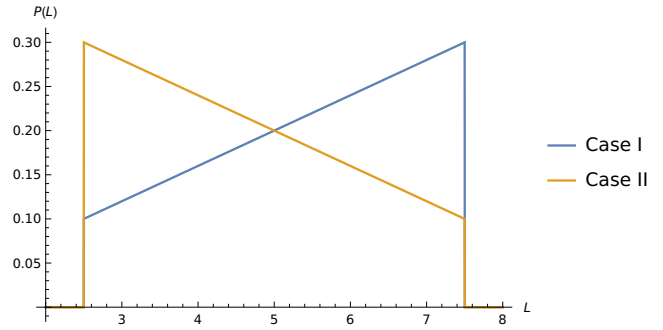

Fig. S3 Asymmetrical probability distributions $P_l(L)$ (used for the polydisperse L and monodisperse D case). We chose to model the L distribution with two probabilities that are not symmetrical with respect to the average value $\bar{L}$ to assess that the asymmetry (or symmetry) in $P_l(L)$ does not have any effect on the value of $\tilde{v}$. As $\bar{L} \neq \bar{A}$, the two L distributions reported are normalised by two different values of D so to grant $\bar{A} = 5$ for both cases.

5 Comparison between theoretical and computational EOS in the nematic phase

For the monodiperse case, the G_L $(PI_L = 0.5)$ and the IG_D $(PI_A = 0.5)$ cases, we calculated the theoretical EOS for the packing fractions corresponding to the nematic phase and compared them with the corresponding computational results, as reported in figure S6.

6 Standard, three-dimensional and orientational distribution functions

In figure S7 the standard, three-dimensional and orientational distribution functions $g(r)$, $g^{3D}(\mathbf{r})$ and $g_2(r)$ are reported to exemplify the emergence of order in the phase space of HSCs with different polydispersities.

The standard radial pair distribution function $g(r)$ is defined as:

$$g(r) = \frac{1}{4\pi\rho r^2 N} \sum_i \sum_{j \neq i} \delta(r - r_{ij})$$

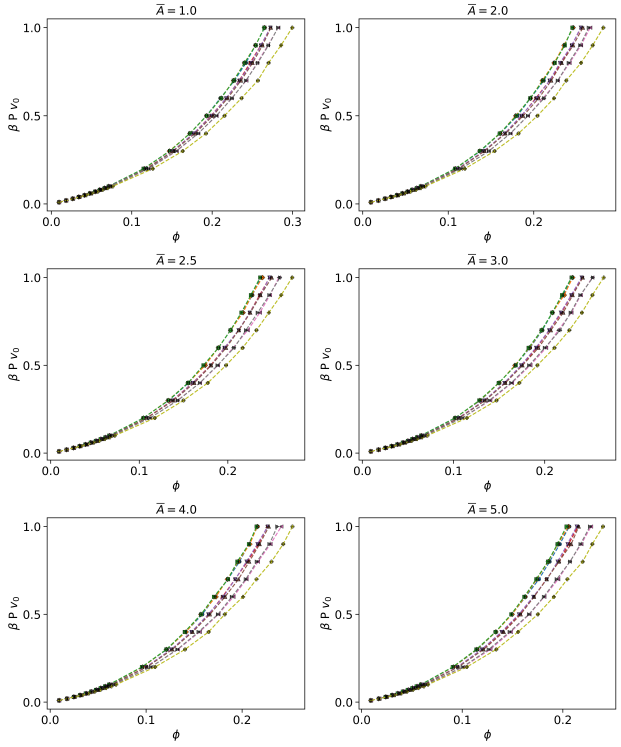

Fig. S4 EOS of the systems for the cases of $\bar{A} = (1, 2, 2.5, 3, 4, 5)$ as computed from MC simulations for the monodisperse (blue circles), G_L $(PI_L = 0.5)$ (orange diamonds), G_L $(PI_L = 0.75)$ (green squares), G_D $(PI_D = 0.5)$ (red crosses), $G_{L,D}$ $(PI_A = 0.5)$ (purple downward triangles), IG_D $(PI_A = 0.5)$ (brown upward triangles), G_D $(PI_D = 0.75)$ (pink leftward triangles), $G_{L,D}$ $(PI_{L,D} = 0.75)$ (gray rightward triangles), and IG_D $(PI_A = 0.75)$ (olive plus symbols).

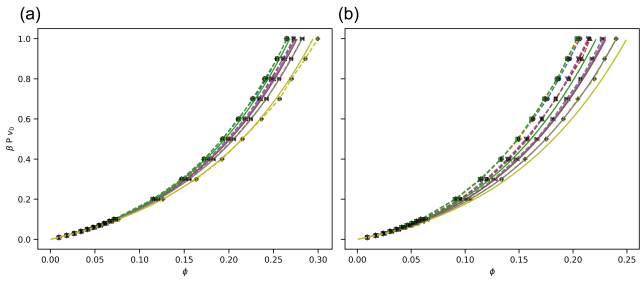

Fig. S5 Qualitative agreement between theory and MC simulations in the case of $\bar{A} = 1$ (a) and $\bar{A} = 5$ (b) for monodisperse (blue circles), G_L $(PI_L = 0.5)$ (orange diamonds), G_L $(PI_L = 0.75)$ (green squares), G_D $(PI_D = 0.5)$ (red crosses), $G_{L,D}$ $(PI_A = 0.5)$ (purple downward triangles), IG_D $(PI_A = 0.5)$ (brown upward triangles), G_D $(PI_D = 0.75)$ (pink leftward triangles), $G_{L,D}$ $(PI_{L,D} = 0.75)$ (gray rightward triangles), and IG_D $(PI_A = 0.75)$ (olive plus symbols). Full lines show Parsons-Lee calculation for the respective system.

where ρ is the density of the system, N is the number of particles, r_{ij} is the modulus of the distance between the center of mass of the particles i and j and $\delta(r - r_{ij})$ is the Dirac function which gives 1 if $r = r_{ij}$.

Analogously, the three-dimensional pair distribution function is:

$$g^{3D}(\mathbf{r}) = \frac{1}{\rho N} \left\langle \sum_{i=1}^{N} \sum_{j \neq i} \delta\left(\mathbf{r} - (\mathbf{r}_i - \mathbf{r}_j)\right) \right\rangle$$

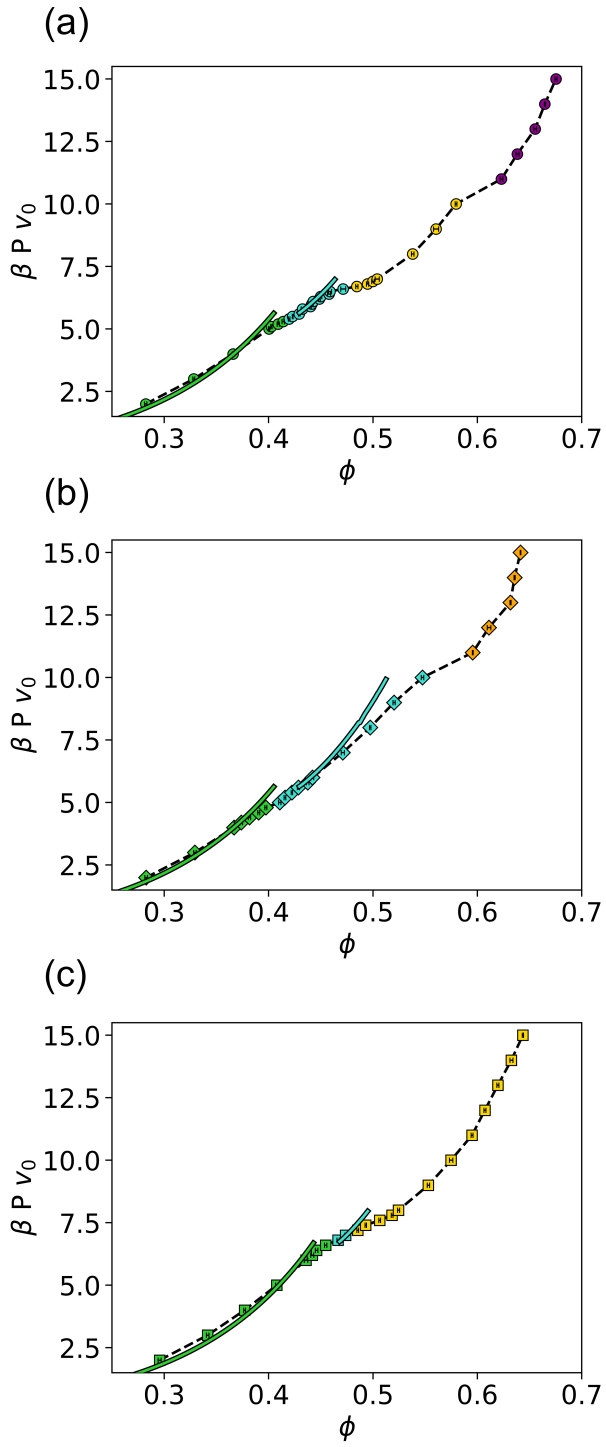

Fig. S6 EOS of the systems in the case of $\bar{A} = 5$ as computed from MC simulations (symbols) and the corresponding theoretical evaluations (full lines) for the monodisperse case (a), G_L $PI_L = 0.5$ (b) and IG_D $PI_D = 0.5$ (d), respectively. The phases are differently colored: Isotropic I (green), Nematic N (cyan), Smectic Sm (yellow), Columnar Col (orange), Crystal K (purple).

When analysing ordered phases, different correlation emerges according to the plane observed. For instance, in the ordered phases, by choosing the z-axis to be parallel to the nematic one,

correlations in planes perpendicular and parallel to it are observed by computing g(x, y, 0) and g(0, y, z), respectively.

The orientational radial pair distribution function $g_2(r)$ unveils an eventual angular correlation between couple of particles as a function of the distance r between their centres of masses:

$$g_2(r) = \langle P_2(\cos(\theta_{ij}(r))) \rangle$$

where P_2 is the second order Legendre polynomial $P_2(\cos(\theta_{ij}(r))) = (\cos^2(\theta_{ij}(r)) - 1)/2$, $\cos(\theta_{ij}(r)) = \boldsymbol{u}_i \cdot \boldsymbol{u}_j$, and $\theta_{ij}(r)$ is the angle between the main axes $\boldsymbol{u}_i$ and $\boldsymbol{u}_j$ of the i-th and j-the particles.

These functions provide information over both the arrangement and alignment of the particles one with respect to the other.

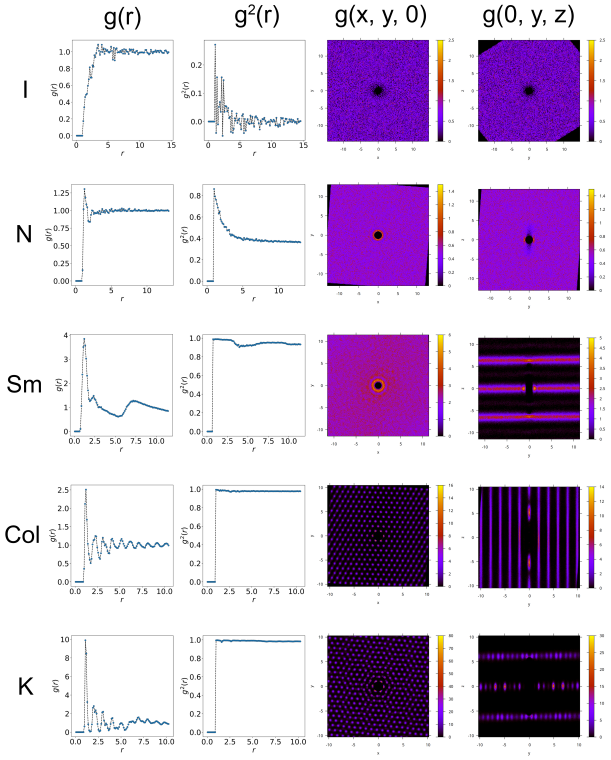

Fig. S7 Standard, three-dimensional and orientational distribution functions $g(r)$, $g^{3D}(\mathbf{r})$ and $g_2(r)$ as resulting from representative MC simulations of HSCs systems in the Isotropic (first row), Nematic (second row), Smectic (third row), Columnar (fourth row), and Crystal (fifth row) phases.

7 Theory comparison

Figure S8 shows the difference $\Delta\phi = \phi_{mono} - \phi_{poly}$ between the equilibrium packing fraction obtained for the monodisperse and all polydisperse cases for $\bar{A} = (1,5)$. From the data is apparent that $\Delta\phi$ is reproduced quantitatively by the theoretical approach for $PI = 0.5$.

Such a quantitative result renders the theoretical prediction a simple and powerful predictive tool. In fact, by having knowledge of the EOS for a monodisperse reference system (as, for instance, obtained from an MC simulation or from literature), by applying the generalised Parsons-Lee theory (Equation 14) with the values of $\bar{v}_0$ and $\bar{v}_{\text{excl}}$ corresponding to the target polydispersity, it is possible to compute the EOS of the polydisperse system. As an example in figure S9, this combined theoretical-computational result is reported for the case of $\bar{A} = 5$ with diameter polydispersity (that is, IG_D and $PI_A = 0.5$). Apparently this result is in excellent agreement with that obtained computationally from the MC simulations of the IG_D and $PI_A = 0.5$ system.

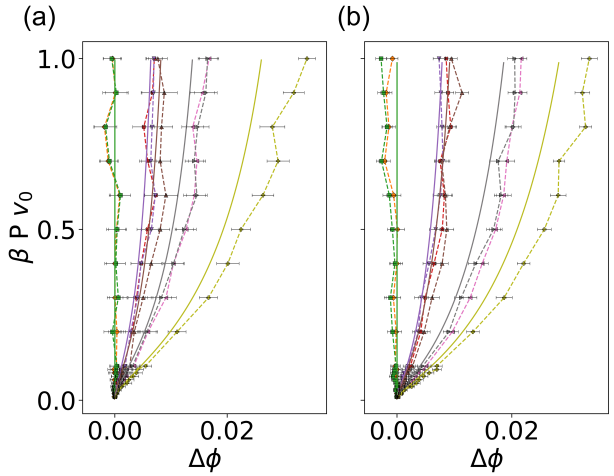

Fig. S8 Quantitative theory agreement. Packing fraction difference $\Delta\phi$ between the polydisperse cases and the monodisperse one for the different systems analysed in this work for $\bar{A} = 1$ (a) and $\bar{A} = 5$ (b). Polydisperse systems are: G_L $(PI_L = 0.5)$ (orange diamonds), G_L $(PI_L = 0.75)$ (green squares), G_D $(PI_D = 0.5)$ (red crosses), $G_{L,D}$ $(PI_A = 0.5)$ (purple downward triangles), IG_D $(PI_A = 0.5)$ (brown upward triangles), G_D $(PI_D = 0.75)$ (pink leftward triangles), $G_{L,D}$ $(PI_{L,D} = 0.75)$ (gray rightward triangles), and IG_D $(PI_A = 0.75)$ (olive plus symbols).

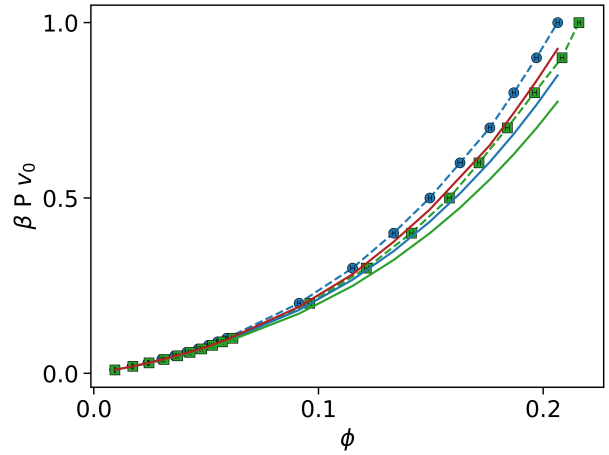

Fig. S9 Theoretical prediction of the EOS of a system with polydispersity in diameter (IG_D system with $PI_A = 0.5$). The reported EOS refer to: the reference monodisperse case obtained either computationally (blue circle) or theoretically (blue line), the system with target polydispersity theoretically obtained (green line), the system with target polydispersity obtained by mean of the combined theoretical-computational approach (red line) and those computationally obtained (green square). The agreement between the last two curves is apparent.

8 Theoretical I-N Transition

Figure S10 shows the I-N theoretical transition computed for all of the polydisperse cases as a function of $\bar{A}$. It clearly appears that the introduction of a length polydispersity does not shift the I-N transition towards higher ϕs in all cases analysed.

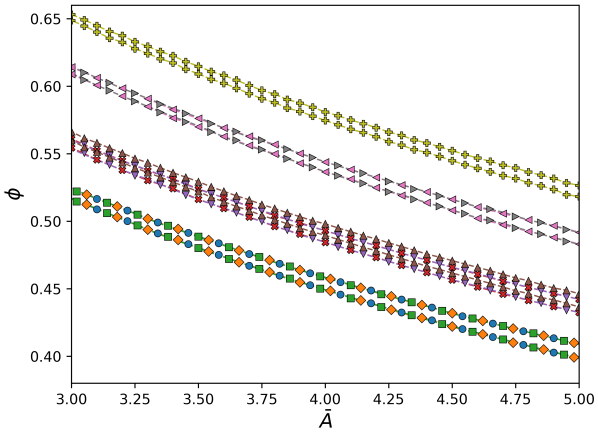

Fig. S10 Theoretical I-N transition as a fuction of $\bar{A}$ for systems: monodisperse (blue circles), G_L $(PI_L = 0.5)$ (orange diamonds), G_L $(PI_L = 0.75)$ (green squares), G_D $(PI_D = 0.5)$ (red crosses), $G_{L,D}$ $(PI_A = 0.5)$ (purple downward triangles), IG_D $(PI_A = 0.5)$ (brown upward triangles), G_D $(PI_D = 0.75)$ (pink leftward triangles), $G_{L,D}$ $(PI_{L,D} = 0.75)$ (gray rightward triangles), and IG_D $(PI_A = 0.75)$ (olive plus symbols).

9 Fractionation Analysis

To assess whether the analysed systems would present any fractionation, we computed the relative probability that two particles with specific L_i and L_j or D_i and D_j are at a given relative distance. To do this we computed probability $g(r, X_i, X_j)$ of finding a particle of kind X_j at a distance r from a particle X_i:

- we chose a specific particle with a specific length $\bar{L}$ amongst the ones defined by the $P_l(L)$ distribution. Defining shells of increasing width centered around the selected particle, we estimate the distribution of particle lengths within each shell. This process has been performed for 7 different lengths $\bar{L}$ for all aspect ratios and all packing fractions (below and above the I-N transition)
- we performed the same calculations for particles having a diameter $\bar{D} \in [D_{\min}, D_{\max}]$. This process has been performed for 7 different lengths $\bar{D}$ for all aspect ratios and all packing fractions (below and above the IN transition)

The distributions gathered through such an approach mirror the length (and/or diameter) distribution defined by $P_d(D)$ and $P_l(L)$ (see respectively fig. S11 and fig. S12). Neither the isotropic phase, nor the nematic one, neither the choice of any specific value for D of for L favours any specific combination of lengths or diameters for given distances between particles. No subclusters that could be identified by a selection of L or D can be identified, thus no significant fractionation can be appreciated in the system.

It is interesting to analyse the behaviour of the orientational distribution function of the whole system, by dividing the differ-

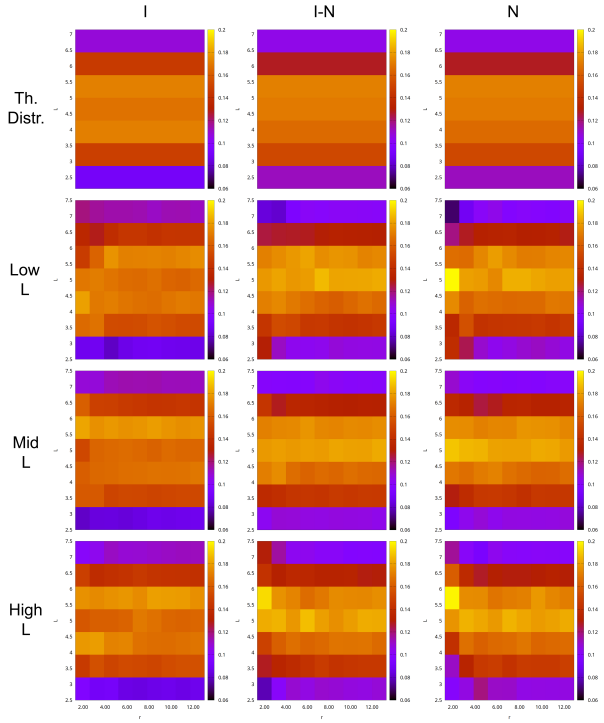

Fig. S11 Probabilities $g(r, L_i, L_j)$ for configurations of polydisperse L systems with $\bar{A} = 5$ in the isotropic phase (left column), around the I-N transition (middle column) and nematic phase (right column). The first row represents the distribution used for generating the initial configuration. To set the L value identifying the particles around which the probability was computed, the L distribution was divided in 7 sub populations. Low L indicates that the particles around which the probability is computed are the ones with the smallest value of L amongst the 7 sub populations; Mid L indicates that the particles around which the probability is computed are the ones with the intermediate value of L ($L_{\mathrm{MID}} = 1/2(L_{\mathrm{LOW}} + L_{\mathrm{HIGH}})$; High L indicates that the particles around which the probability is computed are the ones with the highest value of L amongst the 7 sub populations chosen.

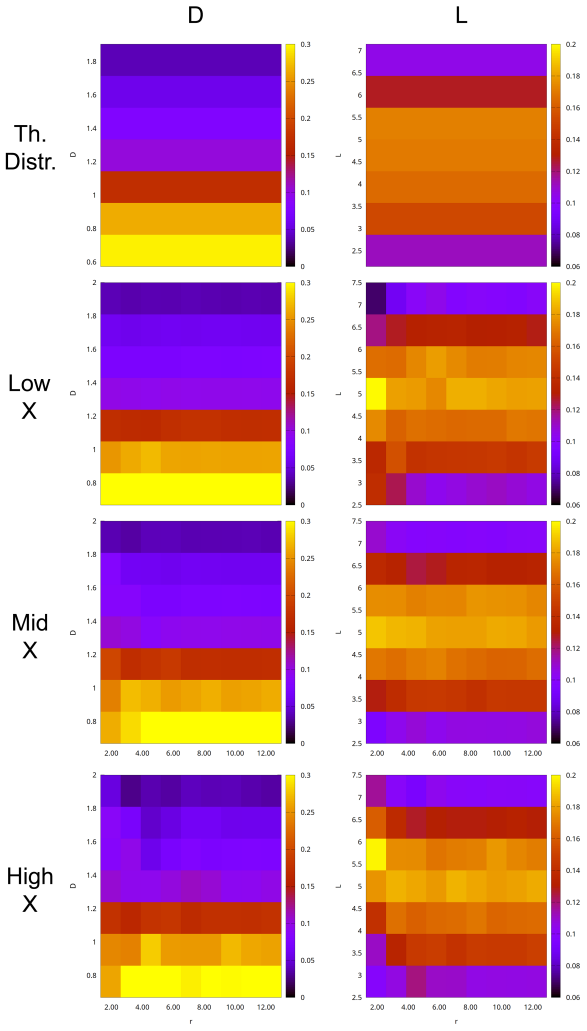

Fig. S12 Probabilities $g(r,X_i,X_j)$ for nematic configurations of polydisperse D (left column) and polydisperse L (right column) systems with $\bar{A}=5$. Each graphic represents the probability to find a particle with a certain value of D or L (y axis) at a given distance r (x axis). The first row represents the distribution used for generating the initial configuration. To set the X value (where X could be either L or D) identifying the particles around which the probability was computed, the X distribution was divided in 7 sub populations. Low X indicates that the particles around which the probability is computed are the ones with the smallest value of X amongst the 7 sub populations; Mid X indicates that the particles around which the probability is computed are the ones with the intermediate value of X ($X_{\rm MID}=1/2(X_{\rm LOW}+X_{\rm HIGH})$; High X indicates that the particles around which the probability is computed are the ones with the highest value of X amongst the 7 sub populations chosen.

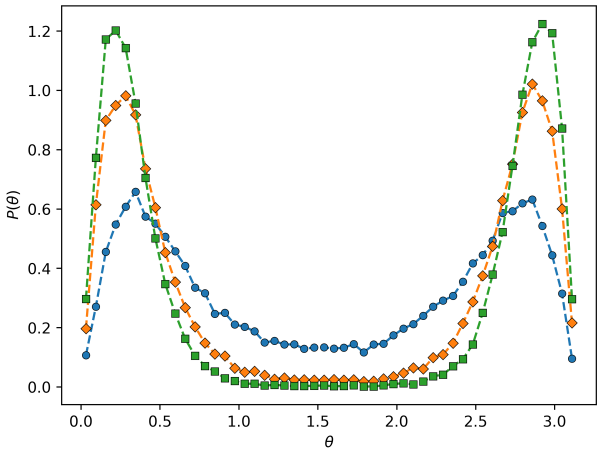

Fig. S13 Probability density for the angle between the main axis of the particles and the nematic one computed for $L_{\rm LOW}$ (blue circles), $L_{\rm MID}$ (orange diamonds), and $L_{\rm HIGH}$ (green squares) for the case $\bar{A}=5$ at the I-N transition ($P^*=6$). The corresponding $\alpha(\bar{D},L)$ are: $\alpha(\bar{D},L_{\rm LOW})=5.30$, $\alpha(\bar{D},L_{\rm MID})=13.32$ and $\alpha(\bar{D},L_{\rm HIGH})=18.93$, while the average value of α computed with the total distribution is $\alpha_{\rm TOT}=12.85$, and the α weighted with the populations of the different particles is $\alpha_{\rm W}=12.60$. With $\bar{D}$ we indicate that all distributions are obtained for a fixed value of D

ent contributions arising from different groups of particles. To identify the sub groups, we proceeded as done for the probabilities reported in Fig.S11 and Fig.S12 i.e. we divided the L (or D) distributions in 7 sub populations. We then considered 3 groups, namely Low L (or D) indicating the smaller value of L (or D) amongst the 7 sub populations; Mid L (or D) is defined as $L_{\rm MID}=1/2(L_{\rm LOW}+L_{\rm HIGH})$; High L (or D) as the particles with the highest value of L (or D) amongst the 7 sub populations chosen.

We hence computed the probability density for the angle between the main axis of the particles and the nematic one for each of the 3 sub groups for L (see Fig.S13), and for D (see FigS13).

It appears immediately that particles defined by smaller values of L as well as smaller values of D (for fixed values of $\bar{A}$) are less aligned to the nematic axis.

Notes and references

1 D. Frenkel and B. Smit, *Understanding Molecular Simulations: From Algorithms to Applications*, Academic Press, ISBN:0122673514, 9780122673511, 2002.

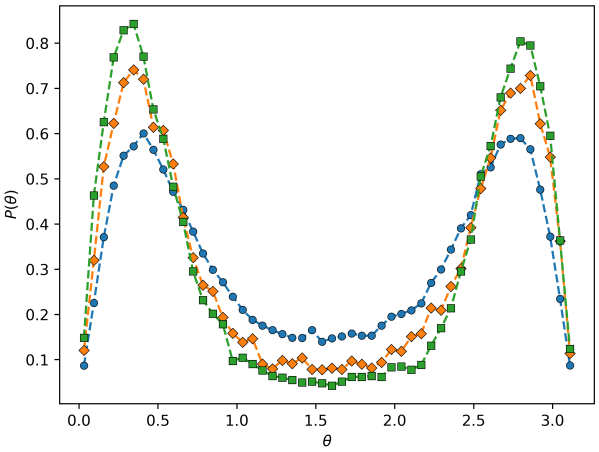

Fig. S14 Probability density for the angle between the main axis of the particles and the nematic one computed for D_{LOW} (blue circles), D_{MID} (orange diamonds), and D_{HIGH} (green squares) for the case $\bar{A} = 5$ at the I-N transition ($P^* = 6.8$). The corresponding $\alpha(D, \bar{L})$ are: $\alpha(D_{\mathrm{LOW}}, \bar{L})) = 4.45$, $\alpha(D_{\mathrm{MID}}, \bar{L})) = 7.21$ and $\alpha(D_{\mathrm{HIGH}}, \bar{L})) = 8.80$, while the average value of α computed with the total distribution is $\alpha_{\mathrm{TOT}} = 5.82$, and the α weighted with the populations of the different particles is $\alpha_{\mathrm{W}} = 5.77$. With $\bar{L}$ we indicate that all distributions are obtained for a fixed value of L